Thesis for the degree of Licentiate of Engineering

Biomass Retrieval in Topographic Boreal Forest using Polarimetric and Tomographic SAR in P- and L-band

Erik Blomberg

CHALMERS

Department of Earth and Space Sciences
Chalmers University of Technology
Gothenburg, Sweden 2017

Biomass Retrieval in Topographic Boreal Forest using Polarimetric and Tomographic SAR in P- and L-band
ERIK BLOMBERG

Radar Remote Sensing
Department of Earth and Space Sciences
Chalmers University of Technology
SE-412 96 Gothenburg, Sweden
Telephone: +46 (0)31-772 1000

Chalmers Reproservice
Gothenburg, Sweden 2017

Biomass Retrieval in Topographic Boreal Forest using Polarimetric and Tomographic SAR in P- and L-band

Erik Blomberg
Department of Earth and Space Sciences
Chalmers University of Technology

Abstract

Forests and their associated habitats are an integral part of Earth's biosphere and provide essential environmental services. There is an ever present need for accurate and economic monitoring of forest parameters such as biomass - of great interest both locally, for forest management and resource utilization, and globally as it represents stored atmospheric CO_2 and one of the largest uncertainties in climate modelling.

Forest monitoring using orbital assets has the benefit of consistent, large scale coverage with short revisit times. Radars have an advantage over optical sensors in that they are active sensors independent of solar illumination and are much less sensitive to weather, with synthetic aperture radar (SAR) providing images comparable to optical data in resolution. The longer wavelengths used by radars interact differently with the forest canopy, with the longest wavelengths able to penetrate down to the ground even in dense forest. Radar backscatter therefore includes information about the forest structure, but may also contain significant contributions from the underlying ground surface.

Electromagnetic modelling of these interactions, the focus of the first paper, is important in order to support the retrieval of relevant parameters from the returned signal. It is demonstrated that much of the variations in intensity and polarization seen in P-band SAR images can be attributed to the direct and indirect reflections of vertical stems on sloping ground. The sensitivity of forest backscatter polarization to the geometry and structure of the scene forms the basis of biomass retrieval models such as the one evaluated in the second paper, which includes all linear polarimetric components as well as a ground slope term. This model, previously evaluated for two Swedish boreal forest sites, is here revisited with a new data set and the results are shown to be consistent with previous findings, although a systematic increase in backscatter attributed to varying moisture conditions result in higher biomass estimates.

The third and final paper includes the first evaluation of biomass retrieval using tomographic SAR (TomoSAR) data representative of a proposed L-band mission with two formation flying satellites. Tomography can resolve the vertical forest profile and offers a new dimension for forest structure investigation. A linear model using the HH-polarized backscatter is found to retrieve forest biomass with an RMSE of 26-30%, performing better than higher resolution data from an airborne SAR despite only utilizing a single polarization.

Keywords: Forest Biomass, SAR, L-band, P-Band, Tomography, EM Modelling

Acknowledgements

I would like to thank my supervisor Lars Ulander for his guidance and advice throughout the writing of this thesis. Thanks to Leif Eriksson for his input as assistant supervisor and group leader, Maciej Soja for showing me the ropes and Johan Fransson and Henrik Persson for making sure I see the trees as well as the forest.

I'm grateful to the rest of the radar group: Albert, Anis, Jan A., Jan T. and Wiebke as well as former members, for being great colleagues and friends. Thank you to everyone at Earth and Space for creating a wonderful environment, not to mention the many interesting discussions.

Most of my work has been funded by the Swedish National Space Board (SNSB) and the European Space Agency (ESA) and I have relied heavily on data and expertise provided through our collaboration with the Department of Forest Resource Management at the Swedish University of Agricultural Sciences (SLU), all of which I greatly appreciate.

Finally, a hug to my family and friends, who I know I can rely on for support when I need it and humorous commentary when I deserve it.

Appended Papers

This thesis is based the following appended papers:

Paper A E. Blomberg, M. J. Soja, and L. M. H. Ulander. "A polarimetric model of topographic effects on P-band forest backscatter". *Proceedings of PolInSAR 2015*. 26-30 January 2015. Frascati, Italy: ESA SP-729, 2015.

Paper B E. Blomberg, M. J. Soja, and L. M. H. Ulander. "Forest biomass retrieval from BioSAR 2010 P-band SAR data using a regression-based model". *2015 IEEE International Geoscience and Remote Sensing Symposium (IGARSS)*. 26-31 July 2015. Milan, Italy, 2015, pp. 4193–4195.

Paper C E. Blomberg, L. Ferro-famil, M. J. Soja, L. M. H. Ulander, and S. Tebaldini. "Forest biomass retrieval from L-band tomography". *IEEE Geoscience and Remote Sensing Letters* (2017). Submitted.

Contents

1 | Introduction

Earth is a planet of trees. Forests cover 31% of the land surface and the trees and plants they contain form an essential part of our biosphere [1]. They clean the air and water from pollutants, prevent soil erosion and absorb rainfall, provide habitats and affect both the local and global climate. Tropical rainforests alone represents 80% of terrestrial biodiversity and 40% of global oxygen production.

Earth is also our home. Humans are changing the face of the planet at a scale and speed orders of magnitude greater than any other species before us. Our use of technology has allowed us to spread to and thrive in all corners of the world and even take our first steps beyond. Our expansion has often been at the expense of forests, which have continued to decline in both acreage and diversity while serving as a source of timber and land. Yet one fifth of the world's population still rely directly on forests for food, water, fuel and income [2].

Forests represent a major part of the living biomass and play an important role in the global carbon cycle, with the greatest short term change in the level of atmospheric CO_2 being the annual variation due to the northern growth season (an effect of the larger proportion of land surface in the northern hemisphere). Forests act as both net sinks and sources of CO_2, depending on conditions and management, with growth and sequestration of dead plant matter in the soil binding carbon and decay, deforestation and fires releasing it. It is estimated that forests absorb 25% of the CO_2 emitted by fossil fuel use [3].

1.1 Forest monitoring

A growing recognition of the environmental services provided by forests has highlighted the need for accurate and economical forest monitoring. Sensors capable of global coverage are preferable, as practices and methods vary and consolidating data sets can be challenging, and using satellites is in practice the only economical way to achieve the coverage and revisit times needed. Many regions with large areas of forest and great need for accurate assessment also lack the resources to perform them.

In-situ measurements of forestry parameters such as stem diameter, height, number density and species generally provide the most accurate data, but involve expensive and time consuming field work and are commonly used for calibration of remote sensing data covering larger areas. Large scale mapping has mostly relied on optical imagery and lidar. However, optical data is limited with regard to how well the forest structure can be characterized, especially for dense forests, and also suffer from a sensitivity to lighting

and weather conditions, especially cloud cover - by definition a significant factor in highly productive rainforests.

Airborne lidar provides high resolution coverage of limited areas, as well as vertical profiles and excellent tree height data, and can be used to extrapolate in-situ data over a larger test site. Lidars operating from orbital altitudes, such as the Geoscience Laser Altimeter System (GLAS) on NASA's Ice, Cloud, and land Elevation Satellite (ICESat), face limitations on resolution and coverage due to the need for high laser power and quality but have nonetheless contibuted significantly to forest research [4].

Another example is the Global Ecosystems Dynamics Investigation (GEDI) lidar, which is to be installed on the International Space Station (ISS) in 2018. GEDI builds on experince with previous lidar missions and is a NASA Earth Venture Instrument specifically designed for forest monitoring. It will acquire 1 m resolution vertical profiles from 25 m diameter spots along 10 parallel tracks separated by 600 m, which will be interpolated onto a 500 m raster with each cell being covered by a few tracks per year. The highest benefit is expected to come from data fusion with sensors having higher resolution and temporal coverage, which will also provide coverage beyond latitudes overflown by ISS ($\pm 51.6°$) [5].

Radars work independently of weather and illumination as they are active sensors using microwaves instead of optical light. High resolution images can be generated with Synthetic Aperture Radar (SAR) and the data downlink bandwidth is often the largest restriction on coverage. However, the interaction between the electromagnetic waves and the forest is not straight forward at these wavelengths which complicates the retrieval of forest parameters from the data. Longer wavelengths penetrate through the canopy, which provides more information from dense forests but also results in contributions from different parts of the forest structure as well as the ground. This is an active research field, with advanced techniques such as polarimetry, interferometry and tomography increasingly being employed and several new missions and sensors are planned for the future[6–8].

1.2 Objectives

The objective of this thesis is to:

- Motivate the need for global forest monitoring and the use of SAR imaging for this purpose.
- Introduce the reader to radar principles needed to understand the benefits and challenges associated with radar based forest monitoring.
- Introduce the more advanced concepts involved in the research that forms the basis for the appended papers.
- Summarize the work and findings presented in the appended papers.

The three appended papers evaluate different models for biomass estimation using satellite based SAR. The first paper focus on simulating and understanding the basic

principles involved in radar scattering of trees, while the second and third papers focus on the retrieval of above ground biomass (AGB), an important parameter for forest management and climate modelling, from SAR images and tomographic radar data.

2 | Radar Remote Sensing of Forests

2.1 Radar

A first hint to what a radar is can be found in the name, which originated as an acronym for RAdio Detection And Ranging [9, 10]. They are devices that can detect the presence of and distance to objects by transmitting radio waves and receiving the reflected signals. First proposed shortly after Heinrich Hertz discovered radio waves in 1886 radars did not see much development until the Second World War, when recognition of their obvious military applications and enabeling technological advances lead to intense research [9]. Today radars are used for everything from tracking asteroids and monitoring weather to helping you park your car [10, 11].

2.1.1 Basic Principles

Modern radars are not restricted to using radio waves. Higher performance electronics and processing has allowed for the use of shorter and shorter wavelengths and most radars operate in the microwave region of the electromagnetic spectrum. Table 2.1 shows the standard used in this thesis for designating the frequency bands.

Many of the names originated as codewords during the early military use of radars and were deliberately chosen not to follow an obvious system [9, 12].

Although the technical details differ depending on the frequency and application all radars operate using the same basic principle: A transmitting antenna sends out a series of pulses that propagate through the air and interact with the environment such that part of the signal is reflected or scattered towards the receiving antenna. The antennas can be located at different positions in what is called a bi-static configuration, but it is more common that they are part of the same physical device or that one antenna alternates between both roles, giving the geometry shown in Figure 2.1. This is known as a mono-static configuration and in this case the distance R to a scatterer is given by Equation 2.1 where T is the time between transmitting and receiving a specific pulse and c is the speed of light [9, 10].

$$R = \frac{cT}{2} \tag{2.1}$$

If a particular scatterer is moving with respect to the radar the corresponding received signal frequency f will be Doppler shifted with the difference, the Doppler frequency f_D,

Table 2.1: IEEE standard letter designations for radar-frequency bands [12]. Note that P-band is not part of the IEEE standard and has been used for several different bands.

Band	Frequency range	Wavelength
HF	3-30 MHz	100-10 m
VHF	30-300 MHz	10-1 m
UHF	0.3-1 GHz	1-0.3 m
L	1-2 GHz	30-15 cm
S	2-4 GHz	15-7.5 cm
C	4-8 GHz	7.5-3.7 cm
X	8-12 GHz	3.7-2.5 cm
Ku	12-18 GHz	2.5-1.7 cm
K	18-27 GHz	1.7-1.1 cm
Ka	27-40 GHz	1.1-0.7 cm
V	40-75 GHz	7-4 mm
W	75-110 GHz	4-3 mm
mm	110-300 GHz	3-1 mm
P	216-450 MHz	1.4-0.7 m

depending on the ratio between the radial component of the relative velocity v_r and the speed of light c as described by Equation 2.2 (for the non-relativistic case).

$$f_D = f\frac{2v_r}{c} \tag{2.2}$$

2.1.2 Scattering mechanisms

The strength of the return signal contains information about the size and physical characteristics of the illuminated scatterers. These properties are combined into the radar cross section (RCS) σ, defined by Equation 2.3 where $\mathbf{E}^i$ and $\mathbf{E}^s$ are the incident and scattered electric fields [9].

$$\sigma = \lim_{R\to\infty} 4\pi R^2 \frac{|\mathbf{E}^s|^2}{|\mathbf{E}^i|^2} \tag{2.3}$$

σ has a unit of m^2. When considering scattering from extended scatterers it is common to use σ^0 which is normalised by the area and has a unit of m^2/m^2.

As the incident wave interacts with an object it is simultaneously scattered, transmitted and adsorbed, with the complex permittivity and surface geometry being the main factors influencing the relative proportions and the resulting spatial distribution. For directional reflectors the RCS can thus be much larger than the physical cross section of the object, with an example being a metallic trihedral corner (retro)reflector with a side length $\gg$ the wavelength.

The size of a scatterer in relation to the wavelength has a large impact on the interaction. Objects where the smallest radius of curvature is $\gg$ the wavelength are

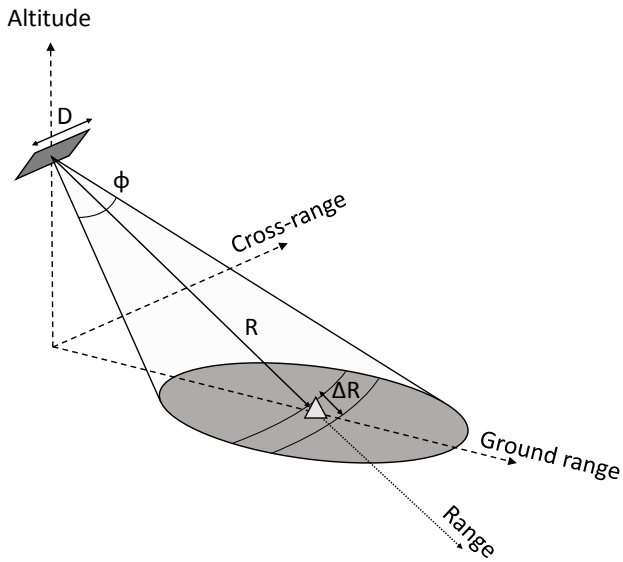

Figure 2.1: *Illustration of the radar geometry. An elevated antenna with an aperture width of D is pointed at an object on the ground (triangle) at radial distance R from the radar.*

adequately described by geometric optics, while the shape becomes less important as the dimensions approaches the wavelength and the strength of the interaction decreases rapidly for objects smaller than the wavelength.

Many radar systems are capable of transmitting and receiving polarized waves so that the incident and scattered electric fields are described by two complex component vectors resulting in four complex scattering components. For example, for linearly polarized waves it is common to use the vertical (V) and horizontal (H) reference planes. If the antenna is capable of transmitting and receiving both separately it can measure the HH, VV, HV and VH contributions and is said to be fully polarimetric. For a mono-static system and passive scene interacting with the incident wave in a linear way reciprocity gives that the two cross-polarized coefficients are identical [13].

Scattering from Trees

A typical tree has a vertical stem rooted in ground with branches, sticks, twigs and eventually leafs or needles extending outwards. This fractal design is evolutionary optimised for collecting sunlight, water and nutrients in competition with neighbouring trees while remaining strong enough to survive winds and precipitation.

Figure 2.2 illustrates how the many orders of magnitude difference in size of the tree elements means that the interaction with an incident electromagnetic wave is greatly dependent on the wavelength. Shorter wavelengths such as C-band and below will interact with the leafs and needles of the canopy, mostly reaching the ground through gaps between trees. Longer wavelengths penetrate into the canopy and interact with the woody parts and even longer wavelengths such as UHF-band and above penetrate through and will

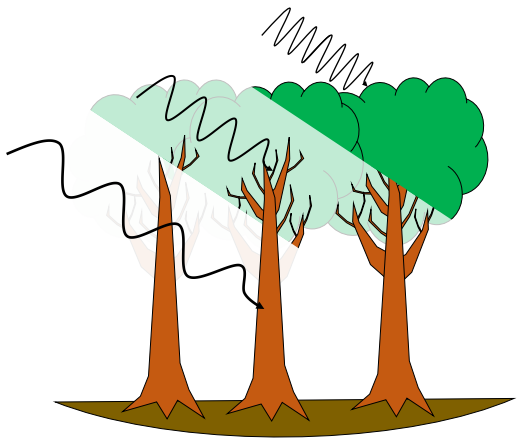

Figure 2.2: *Different wavelengths interact differently with the forest - short wavelengths are scattered and absorbed by the canopy while longer wavelengths penetrate deeper and interact with branches and stems.*

mostly "see" the stems and the ground beneath.

Several different scattering mechanisms will contribute to the return signal as shown in Figure 2.3. There is direct backscatter from the canopy, stems and ground as well as components that have undergone multiple reflections such as from the ground to the tree and back to the antenna (or vice versa). The 90° double bounce between vertical stems and horizontal ground is often a significant component in forest backscatter, especially for longer wavelengths and/or sparse forest.

Polarimetry can be a powerful tool in separating these different contributions. Forest typically have strong cross polarized signatures at shorter wavelengths due to the random orientation of twigs and leafs in the canopy. The ground-stem double bounce will also result in cross polarization on sloping ground and this mechanism is therefore sensitive to the local topography.

2.1.3 Resolution

How precisely a radar can measure the distance to an object, the range resolution ΔR (see Figure 2.1), is directly determined by the duration τ, or, equivalently, the bandwidth B of the transmitted pulses as given by Equation 2.4. It is common to use frequency modulation (such as a chirp) to increase pulse bandwidth in order to improve resolution instead of shortening pulse duration as this would require high power and high voltage electronics.

$$\Delta R = \frac{c\tau}{2} = \frac{c}{2B} \tag{2.4}$$

Pointing of the antenna will give the azimuth (horizontal) and elevation (vertical) angles for a specific scatterer. As in optics, the angular beamwidth ϕ is limited by the size

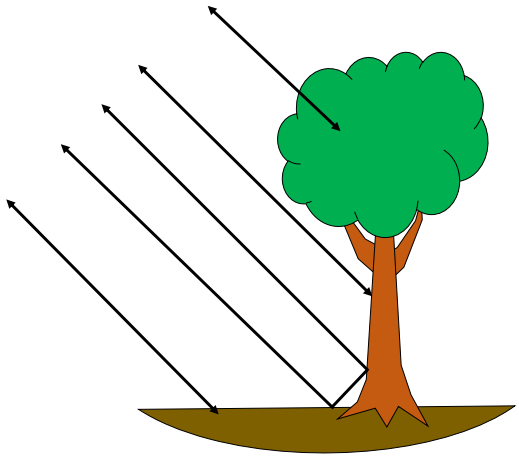

Figure 2.3: *Scattering mechanisms illustrated by a tree: A part of the incident wave is directly scattered back from the surface of the stem or ground while another part undergo multiple reflections. Backscatter from the crown volume is heavily dependent on wavelength and tree structure.*

D of the aperture due to diffraction, with Equation 2.5 being a common approximation for $D \gg \lambda$.

$$\phi \approx \frac{\lambda}{D} \tag{2.5}$$

The small angle approximation then results in a range-dependent cross range resolution ΔCR as given by Equation 2.6.

$$\Delta CR \approx R\Delta\phi \approx \frac{R\lambda}{D} \tag{2.6}$$

Practical limitations on antenna size and longer wavelengths (as compared to optical sensors) result in the resolution generally being much worse in cross-range compared to range, especially for large ranges. This might not be a problem for target tracking, as the distance and radial velocity can be accurately determined, but it is a major drawback for imaging applications.

2.2 Synthetic Aperture Radar

First proposed in 1951 by C. A. Wiley [14] and rapidly implemented and developed during the 1950s, SAR is a method to improve cross-range resolution beyond the limits set by the physical antenna. If the radar is implemented as coherent system, i.e. records both the amplitude and the phase of the return signal, measurements from different positions can be coherently added together to produce results equivalent to a larger antenna (as is done with phased arrays).

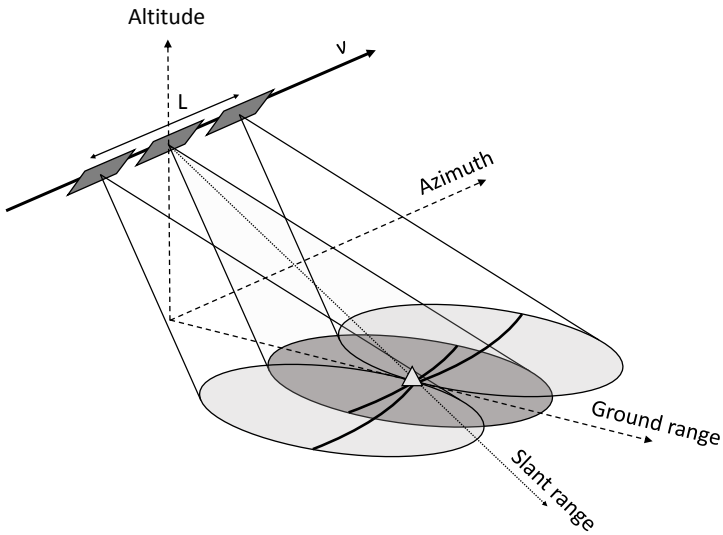

Figure 2.4: *Illustration of a (right) broadside looking stripmap SAR implementation of the geometry shown in Figure 2.1. The antenna illuminates the ground at a fixed orientation while moving perpendicularly at a constant velocity v along the azimuth axis. L is the length of the synthetic aperture used for imaging.*

Figure 2.4 is a basic example of SAR - a single antenna is moved with constant velocity v while taking measurements over a synthetic aperture of length L. The antenna and radar beam are fixed with regard to the platform and are continuously imaging or mapping a strip of the surface - this is known as "stripmap" mode.

2.2.1 SAR Resolution

Replacing the real aperture of length D with a linear synthetic aperture of length L will improve the azimuth resolution according to Equation 2.6. A detailed analysis treating the synthetic aperture as a phased array [15] or, equivalently, considering the Doppler shifting of the frequency as a scatterer moves through the beam [9] results in Equation 2.7 for a broadside looking SAR.

$$\Delta CR = R\Delta\phi_{SAR} \approx \frac{R\lambda}{2L} \tag{2.7}$$

The resolution of a synthetic aperture is thus improved by a factor 2 compared to that of a real aperture of the same length. The physical explanation is that the radar measures the signal separately for each position in the synthetic aperture before coherent summation, thereby involving the two-way range difference for each pair, while the real aperture only involves the one-way difference from the scatterer to the antenna [15].

For a stripmap acquisition such as depicted in Figure 2.4 the maximum length L of the synthetic aperture is determined by the width of the beam given by Equation 2.5.

Insertion into Equation 2.7 results in Equation 2.8.

$$\Delta CR = \frac{D}{2} \tag{2.8}$$

Eliminating the range dependence means that even orbital platforms can achieve azimuth resolutions on the order of meters, often being limited by the range resolution set by available bandwidth instead. The resolution chosen involves secondary considerations such as the need for larger antennas to get a sufficient signal to noise ratio and the need to store and transmit the resulting large data volumes.

Resolution is often traded for coverage as many SAR systems use steerable antennas. ScanSAR mode scans the beam, covering a larger area but illuminating each patch for a shorter time decreasing resolution. Moving the beam (or following a curved trajectory) to focus on a small area of interest results in a longer synthetic aperture, increasing resolution beyond the limit set by Equation 2.8 in what is known as spotlight mode.

2.2.2 SAR Images

Processing SAR data into images is computationally intensive, in large part due to the scene being in the near field region of the synthetic aperture. This could originally only be achieved with optical processors but modern implementations use digital processing with few exceptions. Several different types of image forming algorithms have been developed, using various simplifying assumptions and often suited for specific geometries [14, 15].

The ideal SAR data from a processing viewpoint would be measurements from equidistant points along a straight line to within a fraction of the wavelength. Orbital platforms approach such an ideal track but it is unrealistic for airborne radars due to air buffeting and manoeuvring. The impact of these deviations can be minimized by using highly accurate inertial measurement units to record the movement of the antenna and compensating during processing. There are also autofocusing algorithms which iteratively focus the image by modifying the estimated track positions.

The result of this processing is generally a single look complex (SLC) image in the slant range-azimuth plane where the magnitude of each complex pixel is proportional to the square root of the radar cross section. It is then common to geocode the image, i.e. project it onto the ground or sea surface to remove geometric distortions and ensure compatibility with common coordinate systems. Multi-looking, i.e. averaging over multiple pixels or closely related images is used to decrease speckle. Speckle is a type of noise unique to coherent systems where interference between strong scatterers below the resolution limit causes random intensity variations in each pixel.

Although SAR images often resemble optical photographs, especially after geocoding and multi-looking, there are important differences to consider when interpreting the information. The radar is the source of illumination and measures distance to the scatterers instead of the angles between them as in an optical system. The apparent viewpoint is therefore located perpendicular to the slant-range azimuth plane and shadows represent a total lack of information. Likewise, points oriented perpendicular to the radar, such as on a steep hillside, will overlap in range. Geocoding might stretch out the corresponding pixels but can not retrieve the lost information.

Figure 2.5: *Geocoded L-band SAR image from Remningstorp in the south of Sweden. Acquired with SEHTI as part of the BioSAR 3 campaign using a bandwidth of* 150 MHz *at* 1.3 GHz. *Resolution is* 0.9 m *by* 0.9 m. *Polarimetric information is included by the use of the Pauli decomposition for the RGB channels: HH-VV (even-bounce), HV (volume scattering), HH+VV (odd-bounce). Courtesy: ONERA.*

Figure 2.5 demonstrates many features typical of monostatic SAR images. Forested areas are bright with a strong volumetric HV component while flat areas such as fields are dark, as most of the incident energy is specularly reflected away from the receiver. The fields have varying polarimetric response depending on orientation of surface features and crop properties. Built up areas are characterized by geometric shapes and strong point like scatterers at corners and edges. The side lobes of strong returns result in streaks in the range and azimuth directions. Some notable features have been annotated:

1. Large barn with a roof oriented perpendicular to the flight track, resulting in a strong single-bounce signal.
2. 5 m trihedral (triple-bounce) used for radiometric calibration.
3. Small lake - still water and pavement are smooth at this wavelength resulting in very low backscatter.
4. Powerlines visible despite their relative thinness (wire diameter $\ll \lambda$) due to the strong coupling with the parallel component of the incident electric field.
5. Farm with several houses giving strong ground-wall double bounce echoes.
6. Overgrown lake with a marked double-bounce from the low vegetation covering most of the surface.

2.3 Interferometry and Tomography

An inherent limitation of SAR is that while range and azimuth are well resolved the beam size remains the only constraint in the third spatial dimension, elevation. This is resolved with the assumption that the measured backscatter originates at the intersection of the slant-range plane and a ground plane. However, accurate projection and geocoding requires a high resolution digital terrain model (DTM) to avoid topographic artefacts. Any features extending from the assumed surface will be distorted and volumetric backscatter will be summed over the slanted resolution cells.

Interferometric SAR (InSAR) uses two antennas, either mounted separately on the same platform or on separate platforms, to create a baseline perpendicular to the SAR track. The difference in phase between the receivers caused by the slight difference in path length can then be used to compute the elevation, or equivalently height, of a scatterer [16]. This can be used to create accurate global DTMs, for example the Shuttle Radar Topography Mission DTM acquired in 2000 using a 60 m boom deployed from Space Shuttle Endeavour and the 2014 WorldDEM$^{\text{TM}}$ based on TanDEM-X data (see section 2.4). InSAR heights data from forested areas can be used to estimate biomass as well as forest changes [8, 17]. The baseline can also be temporal, i.e. following the same track at a later date to determine changes in elevation. This enables large scale monitoring of seismic and volcanic activity as well as movement of ground water and ice sheets.

Tomographic SAR (TomoSAR), illustrated in Figure 2.6, is the generalisation of InSAR onto multiple baselines, resulting in multiple resolution cells in elevation. This is an

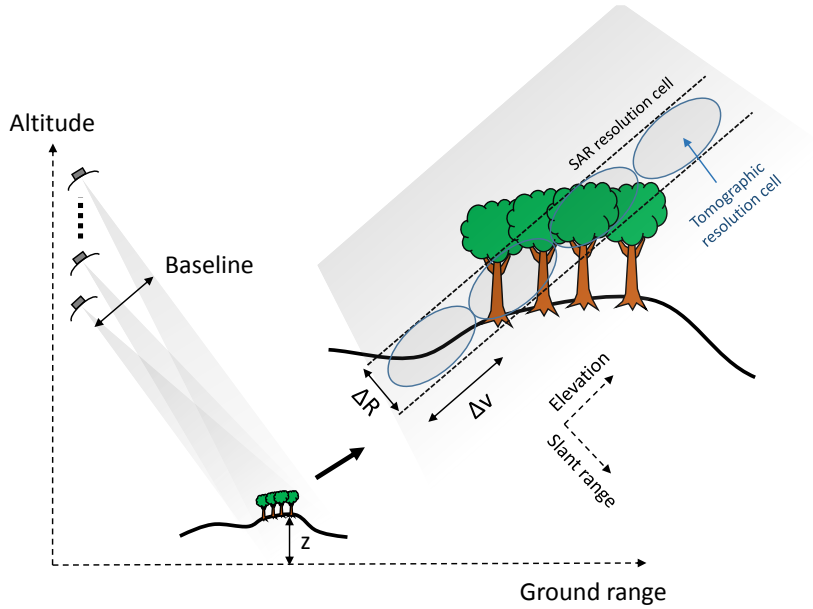

Figure 2.6: *Tomographic SAR geometry viewed along the azimuth axis. Antennas flying in formation or on repeated passes with a vertical separation create a tomographic baseline perpendicular to the slant range-azimuth plane.*

extension of the synthetic aperture methodology in two dimensions, thereby resolving the imaged scene in tree dimensional space (range being the third) [18]. The same principles apply, however there are several factors that can make tomography challenging in practice. A SAR requires that the radar system and the scene maintains coherence during the synthetic aperture, which is on the order of seconds to minutes for airborne platforms and seconds for satellites. The time between the tracks making up the different tomographic baselines is much longer, up to several days for orbital sensors. It is thus only possible to perform tomography for persistent scatterers that do not decorrelate between passes, which would limit its use for forest applications to the longest wavelengths. However, a work around is possible using single-pass InSAR data. An InSAR acquisition using a certain baseline corresponds to a specific vertical wavenumber and a tomographic reconstruction can therefore be made from multiple InSAR passes at varying baselines.

The limited vertical extent of most scenes means that TomoSAR can provide useful resolution even with a relatively small number of baselines. Being able to distinguish between backscatter from the ground and different parts of the vertical forest profile is very useful with regard to forest monitoring and several airborne campaigns have collected data suitable for tomographic processing. Upcoming and proposed missions such as BIOMASS, TanDEM-L and SAOCOM-CS all have proposed tomographic acquisition modes, specifically targeting forest measurements.

2.4 Current and future satellite missions

Satellites take many years to plan, build and launch and this is especially true for one-off scientific missions. The first civilian SAR satellite was the L-band Seasat launched by NASA in 1978. Deemed a great technical and scientific success, despite failing after only 110 days on orbit, Seasat paved the way for steady progression of more and more capable orbital SARs [19]. This section contains some examples of current and future missions with relevance to forest monitoring. Resolution and coverage are best possible performance and are generally obtained using different modes (see subsection 2.2.1).

Current

Sentinel 1, currently comprised of 1A and 1B but to be joined by 1C and 1D, are the SAR segment of ESAs Copernicus Program. Launched into a 693 km sun-syncronous orbit (SSO) in 2014 and 2016 respectively they are identical C-band (5.405 GHz) dual polarized SAR capable of 5 m by 5 m resolution and a max swath width of 400 m and a revisit cycle of 12 days per satellite [20].

ALOS-2, JAXAs follow on to ALOS, is equipped with the PALSAR-2 L-band (1.2 GHz) SAR. Launched into a 628 km 14 day repeating SSO in 2014 it can acquire fully polarimetric data and has a maximum resolution of 3 m in range by 1 m in azimuth and a swath width of up to 490 km [21].

TanDEM-X is a twin satellite constellation consisting of the original TerraSAR-X (launced 2007) and its sister satellite TanDEM-X (launched 2010). They fly in close formation in a 514 km SSO and can operate their X-band (9.65 GHz) SARs in both dual monostatic, bistatic and interferometric modes. Max resolution is 1.7 m in range by 0.24 m in azimuth and maximum swath width is 266 km. The primary mission has been the generation of a global 12 m gridded DTM with a relative and absolute error less than 4 m and 10 m respectively [22].

Future

NISAR, a collaboration between NASA and ISRO, will be the first dual frequency (L- and S-band at 1.2 GHz and 3.2 GHz) orbital SAR when it launches in 2020. Having fully polarimetric InSAR capability and operating from a 747 km SSO, it is intended to monitor a number of environmental variables ranging from Arctic and Antarctic sea ice to coastal winds and forest biomass [23].

SAOCOM-CS is a proposed passive ESA companion satellite to the National Commission for Space Activities of Argentinas (CONAEs) upcoming SAOCOM 1B L-band SAR mission. The aim of the companion satellite is to extend the fully polarimetric and interferometric SAOCOM mission with bistatic and specular acquisition geometries as well as a tomographic mode. The resolution would be set by the active satellite at 10 m in range by 6 m in azimuth [24].

BIOMASS is ESAs seventh Earth Explorer Mission and will be the first orbital P-band SAR mission implemented, having a permit to operate as a secondary user at 435 MHz. Specifically targeting forest monitoring BIOMASS will be fully polarimetric, with an aim for better than 60 m in range by 50 m in azimuth resolution and have both SAR, InSAR and TomoSAR modes (repeat pass) [25].

TanDEM-L builds on the success of TanDEM-X and will have two identical formation flying L-band SAR satellites. Under development by DLR, they are envisioned to be fully polarimetric with maximum resolution of about 2.5 m in range by 7 m in azimuth and maximum swath width of 350 km [26].

3 | Summary of Appended Papers

This chapter summarizes the appended papers.

3.1 Paper A: Polarimetric modelling of topography-stem interactions at P-band

P-band waves penetrate through the forest layer and the interaction between reflections of the ground and the stems greatly affect total backscatter. Especially the double bounce mechanism is sensitive to the local topography, which has to be taken into account for accurate biomass retrieval [7, 27–30]. This paper investigates the effects of a varied topography on forest backscatter at P-band through electromagnetic simulations.

A Cylinder-Over-Ground model from [31] was chosen with the aim to enable detailed geometries with individual trees while keeping the computational requirements low, i.e. running the code on a standard PC. Each tree is modelled as a stack of 10 dielectric cylinders placed on an infinite dielectric ground plane, with cylinders and planes independently scaled and oriented to fit the scenario. The simulation provides fully polarimetric backscatter components corresponding to the direct, double and triple bounce scattering mechanisms and generates a SAR image.

Three scenarios are presented with the first being a forest of randomly placed trees on a symmetric conical hill with a slope of 20°. The other two scenarios uses in-situ tree and topography data from two 80 m by 80 m forest plots at the Remningstorp test site, aquired during the BioSAR 3 campaign [32]. The simulation confirms the expected impact of sloping ground and accurately captures the spatial variation caused by the topography at Remningstorp. Results show the backscatter intensity variations have high contrast, most likely due to the lack of both ground backscatter and attenuation in the canopy in the model. Future modelling will benefit from including a direct scattering mechanism for the ground surface as well as more vegetation elements such as branches.

3.2 Paper B: Biomass retrieval from P-band SAR data using a regression-based model

Paper B revisits the results of [7, 33], which presented biomass retrievals at P-band using the model described by Equation 3.1 where B is the biomass, γ^0_{PQ} are the different

polarimetric components of projected and normalized backscatter γ^0 and u is the surface slope, i.e. the angle between the ground normal and vertical. The HV backscatter coefficient shows a high correlation with biomass while the ratio of the HH and VV components compensates some of the biomass-independent factors such as moisture, forest structure [34], with the ground slope included to further mitigate topographic effects.

$$\log_{10} B = a + b \cdot [\gamma^0_{HV}]_{dB} + c \cdot [\frac{\gamma^0_{HH}}{\gamma^0_{VV}}]_{dB} + d \cdot u \cdot [\frac{\gamma^0_{HH}}{\gamma^0_{VV}}]_{dB} \tag{3.1}$$

This model was previously evaluated using data from the BioSAR 1 and Biosar 2 campaigns at Remningstorp (2007) and Krycklan (2008) respectively [7]. This work recreates these results and adds data from BioSAR 3 acquired in 2010 [32]. It is found that the conclusions still hold and that the model is able to highlight changes such as those caused by tree harvest. The most recent data does show a shift toward higher backscatter values relative the older data, resulting in a corresponding increase in modelled biomass. This is most likely due to a higher moisture content and shows that the model is not able to fully compensate for varying water content.

3.3 Paper C: biomass retrieval from tomographic L-band data

Tomographic synthetic aperture radar (TomoSAR) resolves the vertical backscatter profile from scatterers distributed over a volume, such as the forest canopy. Paper C evaluates the use of L-band TomoSAR data to improve boreal forest biomass retrievals by separating the backscatter contributions from the canopy from those originating from ground level.

Two tomographic data sets were generated from L-band SAR data acquired with the airborne E-SAR system specifically for this purpose during the BioSAR 2 campaign [35, 36]: One using the full performance of E-SAR and the second having a reduced bandwidth and parameters corresponding to SAOCOM-CS, a proposed joint CONAE and ESA tomographic L-band (1.275 GHz) SAR satellite mission [24]. The volumetric backscatter, I_{vol}, is defined as the backscatter at and above 10 m and fitted to biomass using a logarithmic transform and a linear model for a single polarization.

A comparison between the TomoSAR retrievals and results obtained using the slope compensated intensity, γ^0, from the corresponding SAR data reveals that tomographic E-SAR data produces the best results at an RMSE of 25% of average biomass, with SAOCOM-CS increasing to 26-30% due to the reduced resolution degrading the vertical backscatter classification. Both tomographic configurations outperform the 2-D SAR retrievals which have an RMSE of 36-39% regardless of resolution as the training plots and validation stands remain adequately resolved. It is concluded that basing forest biomass retrievals on SAOCOM-CS TomoSAR data would offer improved performance over airborne L-band SAR data despite the reduction in available bandwidth.

4 | Conclusions and Future Work

4.1 Conclusions

The work presented in this thesis are all different aspects of the same theme - retrieving forest parameters from remote radar sensing data. Paper A considers the interaction between the incident electromagnetic wave and the forest structure at P-band. It is shown that a Cylinder-Over-Ground model produces the expected results for a test geometry and reproduces general features of polarimetric SAR images using in-situ forest data. P-band backscatter is heavily affected by topography due to the double-bounce between vertical stems and sloping ground. However, a more detailed model is needed to fully reproduce all components of the measured scene.

A previously presented model for forest biomass retrieval from P-band SAR data was evaluated using a temporally expanded data set. The model incorporates a polarimetric ground slope correction and was found to be valid for the new data. However, some systematic shifts were observed revealing that the model is not able to fully eliminate the sensitivity to factors such as moisture content.

Using TomoSAR to obtain the vertical distribution of backscatter can improve parameter retrieval from volumetrically distributed elements in the scene, such as forest canopies. Simulated L-band data corresponding to the configuration of the proposed tomographic SAOCOM-CS satellite result in improved forest biomass retrievals compared to airborne data, even though the orbital sensor has a lower bandwidth. The ability of TomoSAR to separate the backscatter contributions from the canopy from those originating at ground level suggest that further improvements in global forest monitoring will be possible with planned and proposed future TomoSAR missions.

4.2 Future Work

All three subjects covered present clear avenues for further investigation. The modelling of Paper A would benefit from a revisit using a model that includes backscatter from the ground and from the canopy, to clarify if these contributions are sufficient to even out the topography dependent variations that are exaggerated by the current model.

The model presented in Paper B, itself an extension of previous work using new data, should be evaluated for other types of forests. Suitable datasets exist from temperate forest where the model should be directly applicable. Tropical forests present a larger

challenge but could also be evaluated to determine the limits of the model.

Finally, some work could be done to expand on and optimize the tomographic parameters used in Paper C. Further insights in the best use of vertical profile information might be obtained by investigating other tomographic data in combination with electromagnetic modelling.

References

[1] Food and Agriculture Organization of the United Nations (FAO). *The Global Forest Resources Assessment 2015*. Rome, Italy, 2016. URL: `http://www.fao.org/3/a-i4793e.pdf` (visited on 03/13/2017).

[2] Food and Agriculture Organization of the United Nations (FAO). *State of the World's Forests*. Rome Italy, 2014. URL: `http://www.fao.org/3/a-i3710e.pdf` (visited on 03/13/2017).

[3] Y. Y. Liu, A. I. J. M. van Dijk, R. A. M. de Jeu, J. G. Canadell, M. F. McCabe, et al. "Recent reversal in loss of global terrestrial biomass". *Nature Clim. Change* vol. 5, no. 5 (2015), pp. 470–474.

[4] S. S. Saatchi, N. L. Harris, S. Brown, M. Lefsky, E. T. A. Mitchard, et al. "Benchmark map of forest carbon stocks in tropical regions across three continents". *Proceedings of the National Academy of Sciences* vol. 108, no. 24 (2011), pp. 9899–9904.

[5] NASA Science Missions. *Global Ecosystem Dynamics Investigation Lidar*. URL: `https://science.nasa.gov/missions/gedi` (visited on 03/14/2017).

[6] M. Santoro, J. E. S. Fransson, L. E. B. Eriksson, M. Magnusson, L. M. H. Ulander, et al. "Signatures of ALOS PALSAR L-Band Backscatter in Swedish Forest". *IEEE Transactions on Geoscience and Remote Sensing* vol. 47, no. 12 (2009), pp. 4001–4019.

[7] M. J. Soja, G. Sandberg, and L. M. H. Ulander. "Regression-based retrieval of boreal forest biomass in sloping terrain using P-band SAR backscatter intensity data". *IEEE Transactions on Geoscience and Remote Sensing* vol. 51, no. 5 (2013), pp. 2646–2665.

[8] H. J. Persson and J. E. S. Fransson. "Estimating Site Index From Short-Term TanDEM-X Canopy Height Models". *IEEE Journal of Selected Topics in Applied Earth Observations and Remote Sensing* vol. 9, no. 8 (2016), pp. 3598–3606.

[9] R. J. Sullivan. *Radar foundations for imaging and advanced concepts*. SciTech Pub, 2004.

[10] M. A. Richards, J. Scheer, and W. A. Holm. *Priciples of modern radar: Vol. I, basic principles*. SciTech Pub, 2010.

[11] S. J. Ostro. "Planetary radar astronomy". *Reviews of Modern Physics* vol. 65, no. 4 (1993), pp. 1235–1279.

[12] IEEE Aerospace & Electronic Systems Society. "IEEE Standard Letter Designations for Radar-Frequency Bands". *IEEE Std 521-2002 (Revision of IEEE Std 521-1984)* (2003).

[13] J.-S. Lee and E. Pottier. *Polarimetric Radar Imaging: From Basics to Applications*. CRC Press, 2009.

[14] C. A. Wiley. "Synthetic Aperture Radars". *IEEE Transactions on Aerospace and Electronic Systems* vol. 21, no. 3 (1985), pp. 440–443.

[15] W. G. Carrara, R. S. Goodman, and R. M. Majewski. *Spotlight Synthetic Aperture Radar: Signal Processing Algorithms*. Artech House remote sensing library. Artech House, 1995.

[16] R. Bamler and P. Hartl. "Synthetic aperture radar interferometry". *Inverse Problems* vol. 14, no. 4 (1998), R1–R54.

[17] M. J. Soja, H. J. Persson, and L. M. H. Ulander. "Estimation of Forest Biomass From Two-Level Model Inversion of Single-Pass InSAR Data". *IEEE Transactions on Geoscience and Remote Sensing* vol. 53, no. 9 (2015), pp. 5083–5099.

[18] A. Reigber, A. Moreira, and S. Member. "First demonstration of airborne SAR tomography using multibaseline L-band data". *IEEE Transactions on Geoscience and Remote Sensing* vol. 38, no. 5 (2000), pp. 2142–2152.

[19] D. L. Evans, W. Alpers, A. Cazenave, C. Elachi, T. Farr, et al. "Seasat — A 25-year legacy of success". *Remote Sensing of Environment* vol. 94 (2005), pp. 384–404.

[20] ESA Sentinel-1 Team. *Sentinel-1 User Handbook*. 2013. URL: `https://sentinel.esa.int/documents/247904/685163/Sentinel-1%7B%5C_%7DUser%7B%5C_%7DHandbook` (visited on 03/14/2017).

[21] JAXA Public Affairs Department. *ALOS-2 The Advanced Land Observing Satellite-2*. 2015. URL: `http://global.jaxa.jp/activity/pr/brochure/files/sat29.pdf`.

[22] G. Krieger, A. Moreira, H. Fiedler, I. Hajnsek, M. Werner, et al. "TanDEM-X: A Satellite Formation for High-Resolution SAR Interferometry". *IEEE Transactions on Geoscience and Remote Sensing* vol. 45, no. 11 (2007), pp. 3317–3341.

[23] P. Xaypraseuth, R. Satish, and A. Chatterjee. "NISAR spacecraft concept overview: Design challenges for a proposed flagship dual-frequency SAR mission". *2015 IEEE Aerospace Conference*. 2015, pp. 1–11.

[24] N. Gebert, B. Carnicero Domínguez, M. W. J. Davidson, M. Diaz Martin, and P. Silvestrin. "SAOCOM-CS – A passive companion to SAOCOM for single-pass L-band SAR interferometry". *EUSAR 2014; 10th European Conference on Synthetic Aperture Radar; Proceedings of*. VDE VERLAG GmbH, 2014, pp. 1251–1254.

[25] F. Hélière, F. Fois, M. Arcioni, P. Bensi, M. Fehringer, et al. "Biomass P-band SAR interferometric mission selected as 7 th Earth Explorer Mission". *EUSAR 2014; 10th European Conference on Synthetic Aperture Radar*. 3-5 June. 2014, pp. 1152–1155.

[26] M. Eineder, I. Hajnsek, G. Krieger, A. Moreira, and K. Papathanassiou. *Tandem-L: Satellite Mission Proposal for Monitoring Dynamic Processes on the Earth's Surface*. Tech. rep. 2016.

[27] J. J. van Zyl, B. D. Chapman, P. Dubois, and J. Shi. "The Effect of Topography on SAR Calibration". *IEEE Transactions on Geoscience and Remote Sensing* vol. 31, no. 5 (1993), pp. 1036–1043.

[28] L. M. H. Ulander, G. Sandberg, K. Folkesson, G. Smith-Jonforsen, and J. E. S. Fransson. "Topographic and Number Density Effects in Forest Observations with P-band SAR". *5th International Symposium on Retrieval of Bio- and Geophysical*

Parameters from SAR Data, Bari, Italy, September 25-28, 2007, ESA, Istituto di Studi sui Sistemi Intelligenti per l'Automazione. 2007, p. CD.

[29] B. Hallberg, G. Smith-Jonforsen, L. M. H. Ulander, and G. Sandberg. "A physical-optics model for double-bounce scattering from tree stems standing on an undulating ground surface". *IEEE Transactions on Geoscience and Remote Sensing* vol. 46, no. 9 (2008), pp. 2607–2621.

[30] D. Ho Tong Minh, T. Le Toan, F. Rocca, S. Tebaldini, M. M. D'Alessandro, et al. "Relating P-Band Synthetic Aperture Radar Tomography to Tropical Forest Biomass". *IEEE Transactions on Geoscience and Remote Sensing* vol. 52, no. 2 (2014), pp. 967–979.

[31] G. Smith-Jonforsen, L. M. H. Ulander, and X. Luo. "Low VHP-band backscatter from coniferous forests on sloping terrain". *IEEE Transactions on Geoscience and Remote Sensing* vol. 43, no. 10 (2005), pp. 2246–2260.

[32] L. M. H. Ulander, A. Gustavsson, P. Dubois-Fernandez, X. Dupuis, J. E. S. Fransson, et al. "BIOSAR 2010 - A SAR campaign in support to the BIOMASS mission". *2011 IEEE International Geoscience and Remote Sensing Symposium (IGARSS)*. Vancouver, Canada, 2011, pp. 1528–1531.

[33] L. M. H. Ulander, G. Sandberg, and M. J. Soja. "Biomass retrieval algorithm based on P-band biosar experiments of boreal forest". *2011 IEEE International Geoscience and Remote Sensing Symposium (IGARSS)*. Vancouver, Canada, 2011, pp. 4245–4248.

[34] G. Smith-Jonforsen, K. Folkesson, B. Hallberg, and L. M. H. Ulander. "Effects of forest biomass and stand consolidation on P-band backscatter". *IEEE Geoscience and Remote Sensing Letters* vol. 4, no. 4 (2007), pp. 669–673.

[35] I. Hajnsek, R. Scheiber, M. Keller, R. Horn, S. Lee, et al. *BIOSAR 2008: Final report*. Tech. rep. 2009.

[36] S. Tebaldini and F. Rocca. "Multibaseline polarimetric sar tomography of a boreal forest at P- and L-bands". *IEEE Transactions on Geoscience and Remote Sensing* vol. 50, no. 1 (2012), pp. 232–246.